PHYSICAL REVIEW D VOLUME 11. NUMBER 9 1 MAY 1975

Characteristics of V^0 and γ production in pp interactions at 205 GeV/c

K. Jaeger, D. Colley,* L. Hyman, and J. Rest
Argonne National Laboratory, Argonne, Illinois 60439†

(Received 2 December 1974)

In an exposure of the Fermi National Accelerator Laboratory 30-in. bubble chamber to a beam of 205-GeV/c protons, we have determined total and differential cross sections for the inclusive reactions $p+p\rightarrow\gamma+X$, π^0+X, $(K^0/\overline{K}^0)+X$, $\Lambda+X$. Invariant distributions in x indicate that for γ, K^0, Λ production, scaling has set in somewhere before 69 GeV. The γ differential cross sections are consistent with the relation $d\sigma/dP_u\,(\pi^0)=\frac{1}{2}[d\sigma/dP_u\,(\pi^+)+d\sigma/dP_u\,(\pi^-)]$ for all P_u, where $P_u=P_L^*$ or $P_\perp$. The differential cross sections for Λ and K^0 production indicate a break in the distribution at $|t-t_{\min}|=1.5\ (\text{GeV}/c)^2$ and $0.5\ (\text{GeV}/c)^2$, respectively. The Λ polarization is found to be $-(0.25\pm0.26)$, consistent with zero throughout the x region.

I. INTRODUCTION

In this paper we present results on K^0 (or $\overline{K}^0$), Λ^0 (including those from Σ^0 decays), $\overline{\Lambda}^0$ (including those from $\overline{\Sigma}^0$ decays), γ, and π^0 production in pp interactions at 205 GeV/c. The data were obtained from a 50 000-picture exposure (0.23 events/μb) of the 30-in. hydrogen bubble chamber to a beam of 205-GeV/c protons at the Fermi National Accelerator Laboratory (Fermilab). Preliminary results for the inclusive reactions

$$p+p\rightarrow\gamma+X, \tag{1}$$

$$p+p\rightarrow(K^0/\overline{K}^0)+X, \tag{2}$$

$$p+p\rightarrow\Lambda+X, \tag{3}$$

and

$$p+p\rightarrow\overline{\Lambda}+X \tag{4}$$

have already been published[1,2] based on analysis of 15 000 pictures. We now give the final results and compare them, where possible, with data at lower energies.

II. SCANNING, MEASURING, AND FITTING PROCEDURES

The film was first scanned for all beam track interactions within a selected fiducial region, on tables giving an approximately life-size image of the bubble chamber. Kinks as well as associated V^0's and γ's were recorded with the interactions. Subsequently, each event was examined in detail by a physicist who made a careful search for any vees appearing to point to a beam-track-interaction vertex or to a secondary decay vertex. This was done on a scan table that could give an image 6× life size. This large magnification was especially useful for finding vees in high-multiplicity events, where frequently a vee was obscured by the forward-going cone of tracks from the production vertex. Approximately 10% of the vees in the experiment were first found on the high-magnification scan, and were very difficult to observe on the life-size image.

To estimate scanning efficiencies, part of the film was rescanned. The single-scan efficiency for finding events was $(98.5\pm1.0)\%$ [except for elasticlike two-prongs having a short stub, for which it was $(94\pm2)\%$]. The efficiency for finding a vee with an event was $(94\pm3)\%$ assuming random scanning losses only. Vees were kept only if they were within a fiducial volume chosen to give on all views at least 10 cm of track from the decay or conversion point to the edge of the illuminated region of the bubble chamber. Each vee and its associated production vertex were measured on conventional film plane digitizers and processed through the reconstruction program TVGP. The 35% of events failing were remeasured on the high-magnification tables, which are equipped with film plane digitizers. Remeasurements were done up to four times if necessary until $\gtrsim 95\%$ gave good TVGP output. Measurements were processed through SQUAW where 3C fits to V^0 decay or to γ conversion to an e^+e^- pair on a proton or electron were attempted. In making the γ fit, a proton or electron with recoil momentum of order 1 MeV/c constrained to be essentially perpendicular to the γ direction was used. This approximates the behavior of real protons and electrons in the γ conversion process.

The total number of vees found was 1366, of which 1272 passed SQUAW and continued onto the data summary tape (DST). Of the remaining 94 unfitted events, 38 were definitely outside the fiducial volume or within a length of $L_{\min}$ or were definitely γ's of momentum < 100 MeV/c ($L_{\min}$ and $P_{\min}$ will be specified later). Hence, there remained 56 unfitted events which had to be distributed to the different hypothesis. Table I shows a detailed classification of these events. By use of opening angle, ionization, momentum of the measurement, and $\pi\mu e$ decays, the unfitted events could be classified as indicated in Table I. In 32 cases, a clear signature could not be put on the vee, mainly because one of the tracks was buried in the forward cone of tracks from the production vertex of the event with which the vee appeared associated. The 32 unidentified events (columns 5 and 6 of Table I) were distributed for cross-section purposes in proportion to the number of measured events in each channel.

The final number of three-constraint fits on the DST was 1459, which, when compared to the 1272 events, indicates the small ambiguity level of the measured events.

TABLE I. Ambiguity pattern of unmeasured events.

Prong No.	γ	K^0	Λ	$K^0, \Lambda, \bar{\Lambda}$	$K^0, \gamma, \Lambda, \bar{\Lambda}$
2	1	···	···	1	1
4	1	···	···	···	4
6	1	1	···	3	2
8	4	1	···	2	···
10	4	1	1	1	4
12	2	1	2	4	4
14	3	···	···	1	2
16	···	1	···	2	···
18	···	···	···	···	1
Total	16	5	3	14	18

III. SELECTION OF $\bar{\Lambda}$ EVENTS

The first column of part (a) of Table II gives the number of 3C $\bar{\Lambda}$ fits found. Of the 11 events ambiguous between $\bar{\Lambda}$, γ, and K^0, we retained the $\bar{\Lambda}$'s only if it was one of two fits with the highest χ^2 probability. The two-way ambiguous events were then selected from the $P_\perp^-$ distribution. (This momentum component is from the negative track of a vee transverse to the vee line of flight.) These distributions show that $P_\perp^{e^-}$ from γ's, $P_\perp^{\bar{p}}$ from $\bar{\Lambda}$'s, and $P_\perp^{\pi^-}$ from K^0's peak around 0.0, 0.101, and 0.206 GeV/c, respectively. From unique event distributions, we found that events with $P_\perp^{e^-}(\gamma) < 0.0125$ GeV/c should be called γ's and events with $P_\perp^{\pi^-}(K^0) > 0.105$ GeV/c should be K^0's. Using these cuts, we obtain the second column of part (a) of Table II. However, these cuts are not adequate yet to obtain a clean sample of $\bar{\Lambda}$'s since the number of true $\bar{\Lambda}$'s is only of the order of a few percent of the γ and K^0 events. Hence, for the remaining ambiguous fits, we then retained as $\bar{\Lambda}$ only those for which the χ^2 probability was three times that of the competing fit. (The results are insensitive to the exact value of the χ^2 probability ratio.) This selection left us with the events quoted in column 3 of part (a) of Table II.

TABLE II. Selection of $\bar{\Lambda}$, Λ, K^0, and γ events.

(a) $\bar{\Lambda}$ events

	No. of 3 C fits	No. fits after ambiguous event selection	No. events after χ^2 probability selection
Unique	10	10	10
Ambiguous with γ	30	1	0
Ambiguous with K^0	15	13	5
Ambiguous with γ and K^0	11	5	0
Total	66	29	15

(b) Selection of Λ, K^0, and γ events.

	Unique fits			Ambiguous fits				
	Λ	K^0	γ	(Λ, γ)	(Λ, K^0)	(γ, K^0)	(γ, K^0, Λ)	Total
Raw No. of 3C fits	133	389	625	27	48	24	11	1257
Selected No. of 3C fits								
for Λ	133	···	···	9	42	···	2	186
for K^0	···	389	···	···	6	0	1	396
for γ	···	···	625	18	···	24	8	675

IV. SEPARATION OF γ's, K^0's, AND Λ's

After events not selected as $\bar{\Lambda}$'s had been put back into the overall event sample, we arrived at row 1 of part (b) of Table II. The numbers correspond to 3C fits.

Part (a) of Table II, column 1, shows that the number of $\gamma\bar{\Lambda}$, $K\bar{\Lambda}$, and $\gamma K\bar{\Lambda}$ ambiguities is approximately six times the number of unique $\bar{\Lambda}$'s. In the Λ sample, the number of ambiguous $\gamma\Lambda$, $K\Lambda$, and $\gamma K\Lambda$ [part (b) of Table II, row 1] fits is 65% of the unique Λ fits. It is clear that the bulk of the $\bar{\Lambda}$ candidates are γ's and K's, which simulate $\bar{\Lambda}$ kinematics. In the case of the Λ's, this question can be quantitatively investigated by examination of the distributions of the momentum component $P_\perp^-$ of the negative track from a vee transverse to the vee line of flight. Distributions of the transverse momentum are shown in Figs. 1(a)–1(c) for the γ, K^0, and Λ events, respectively. The events in these plots all satisfy suitable fiducial volume cuts as well as minimum decay length criteria. Fast K's and Λ's which are too far into the forward hemisphere are also removed. (These cuts will be discussed in more detail below.) These distributions in Fig. 1 are for unique γ, K, and Λ fits and also for γ, K, and Λ fits ambiguous with others. To a good approximation, all γK and $\gamma\Lambda$ (or $\gamma\bar{\Lambda}$) ambiguities can be resolved by taking the γ fit if $P_\perp^{e^-} < 0.0125$ GeV/c. The percentage of true K or Λ fits lying within this γ selection range can be calculated using the fact that isotropic decay of a vee in its own rest frame gives a probability distribution for $P_\perp^-$ of

$$N(P_\perp)dP_\perp = \frac{P_\perp}{P^*}\,\frac{dP_\perp}{(P^{*2}-P_\perp^{\,2})^{1/2}}\,, \quad 0 \le P_\perp \le P^* \qquad (5)$$

where $N(P_\perp)$ is the fraction of the total number of events expected between $P_\perp$ and $P_\perp + dP_\perp$. P^* is the magnitude of the center-of-mass momentum of the particles from the vee decay ($P^* = 0.1004$ GeV/c for Λ and $\bar{\Lambda}$ and 0.206 GeV/c for K). Integrating Eq. (5) over the $P_\perp$ range used for selection of γ's shows that 0.8% of the Λ's and 0.2% of the K's lie in this interval. Using the number of events in the last column of part (b) of Table II, we find that the ratios of Λ/γ and K^0/γ equal 0.28 and 0.59, respectively. Thus, we estimate that

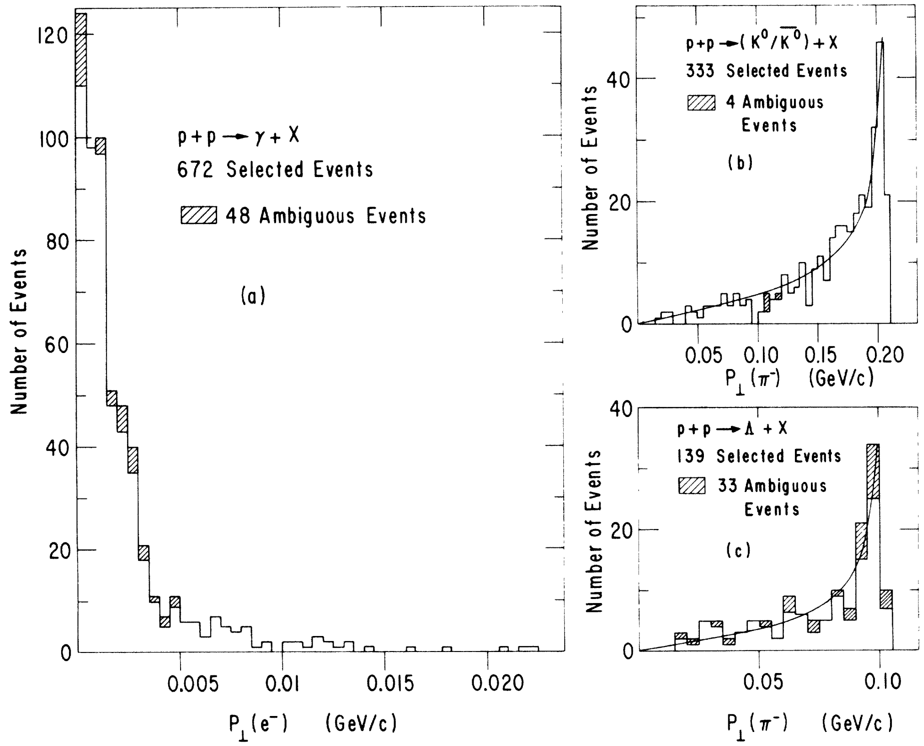

FIG. 1. (a) $P_\perp(e^-)$ of all selected γ events after fiducial volume and $L_{\rm min}$ cuts. (b) Same as (a) for $P_\perp(\pi^-)$ of K^0 events. The curve represents a fit to the probability distribution (see text) normalized to events with $P_\perp(\pi^-) > 0.110$. (c) Same as (a) for $P_\perp(\pi^-)$ of Λ events. The probability curve is normalized to all events.

the γ fits obtained as described are at least 99.7% pure.

Part (b) of Table II also shows an excess of K-Λ ambiguities over K-$\bar{\Lambda}$ ones, suggesting in this case that the ambiguous K-Λ events are primarily Λ's. Integration of the $P_\perp^-$ distribution for K's from 0 to 0.105 shows that ~14% of the K^0's decay in this momentum range. There are 340 unique K's with $P_\perp^{\pi^-} > 0.105$ GeV/c, so there should be 55 K^0 events below; cf. 45 actually found. This once again suggests that most ambiguous Λ/K fits are really Λ's.

The number of ambiguous K/Λ fits [part (b) of Table II, row 1] is 26% of all Λ fits (after all ambiguous γ's have been resolved). The ambiguity is resolved simply by assigning events with $P_\perp^{\pi^-}(K^0) \geq 0.105$ GeV/c to the K^0 channel and those with < 0.105 GeV/c to the Λ's. These selections result in the event pattern shown in part (b) of Table II. The histograms of Figs. 1(a)–1(c) show only these selected events with additional cuts (to be discussed below). We have fitted curves of the form in Eq. (5) to the K^0 and Λ distributions [Figs. 1(b) and 1(c)]. In the K^0 case, the curve was normalized to the events with $P_\perp^{\pi^-} > 0.110$ GeV/c. In both cases, smooth fits to the data are obtained. It is evident from Fig. 1(b) that ~7 events were lost from the K^0 sample into the Λ events. Thus for cross-section purposes, we added 7 events to the K^0's and subtracted them from the Λ sample. We have carefully checked that our selection procedure does not introduce errors which are comparable to the statistical errors of the present experiment. If we changed our selection procedure and chose 7 or 8 Λ events to be K's, we find that the K's so chosen tend to distribute themselves in any given plot (i.e., they do not all pile into a single bin) and the Λ's are removed in a distributed fashion. Hence, the plots do not show any important quantitative changes.[3]

V. FIDUCIAL VOLUME CUTS AND MINIMUM LENGTH

To ensure that all vees have a reasonable potential path length and adequate lengths of decay tracks, fiducial volumes were used both for the production and for the decay vertices. The cuts made were similar to, but slightly more restrictive than, the cuts made at the scanning stage and, in addition, included cuts to remove vees too close to the chamber glass window. Table III gives the number of vees selected into each hypotheses. The first column indicates the final number after all ambiguities have been resolved. The second column gives the number of events remaining after the fiducial volume cut.

To check for loss of vees close to the production vertex, plots were made of the numbers of events of various kinds versus decay length L. These are shown in Fig. 2(a) for unique and ambiguous Λ events, Fig. 2(b) for unique and ambiguous K^0 events, and Fig. 2(c) for unique and ambiguous γ events. The distributions for the K's and Λ's should, of course, rise as $L \to 0$, while that for γ's should be flat (until L gets so big that the limiting effect of the fiducial region becomes important). The distribution for the unique K and Λ events shows a loss of events at $L \leq 1$ cm, while that for the ambiguous K/Λ events and that for the γ's show losses at $L \lesssim 4$ cm. The nature of the losses can be qualitatively understood since the γ's and ambiguous K/Λ events have small opening angles and so are more difficult to separate from the forward cone of charged tracks near the production vertex than are unique K's and Λ's, which tend to be slower and to have larger opening angles. The events remaining in each category after a minimum length cut are given in the third column of Table III. ($L_{\min} = 1.0$ cm for K^0's, unique Λ's; $L_{\min} = 4.0$ cm for ambiguous Λ's and all γ's.)

In order to allow for loss of V^0's near the pro-

TABLE III. Number of $\bar{\Lambda}$, Λ, K^0, γ events after various cuts.

Events	After selection	After fiducial volume cut	After length cut	After forward/backward cut[a]	Average weight
$\bar{\Lambda}$	15	13	13	11	2.36
Λ	186	172	157	139	1.56[b]
K^0	396	373	361	333	1.42[b]
γ	675	624	572	558	56.7

[a] For $\bar{\Lambda}$'s and Λ's, we only take the backward hemisphere events. For K^0's, we only retain events up to $P_L^*(K^0) = 0.4$ GeV/c. For γ's, we cut all events with $P_{\text{lab}}(\gamma) \leq 100$ MeV/c.

[b] Includes correction for K^0 losses into Λ sample and vice versa.

duction vertex and outside the decay fiducial volume, each V^0 remaining after the above cuts was given a weight

$$w = 1/(e^{-L_{\min}/L_0} - e^{-L_{\rm pot}/L_0}, \tag{6}$$

where $L_{\min}$ is the minimum length appropriate to the type of V^0, $L_{\rm pot}$ is the potential path along the V^0 direction from the production vertex to the edge of the fiducial volume, and

$$L_0 = \frac{p}{m} c\tau . \tag{7}$$

In Eq. (7), m and τ are respectively the V^0 mass and lifetime and p is the measured momentum.

Weights for γ's were also calculated using Eq. (7), but with L_0 equal to the interaction length in liquid hydrogen for a γ of given momentum. This length was computed using the table of cross sections given by Knasel.[4] In order to check the weighting procedure, we plotted the number of weighted events versus the minimum length. The results are shown in Figs. 3(a)–3(c) for the K^0, Λ, and γ events, respectively. In the case of the K^0's, we used only unique events with center-of-mass longitudinal momentum component P_L^* < 0.2 GeV/c. For the Λ events, only unique events in the backward center-of-mass hemisphere were employed. With a correct weighting procedure, the distributions should level off after a certain length cut. Within errors, our minimum-length

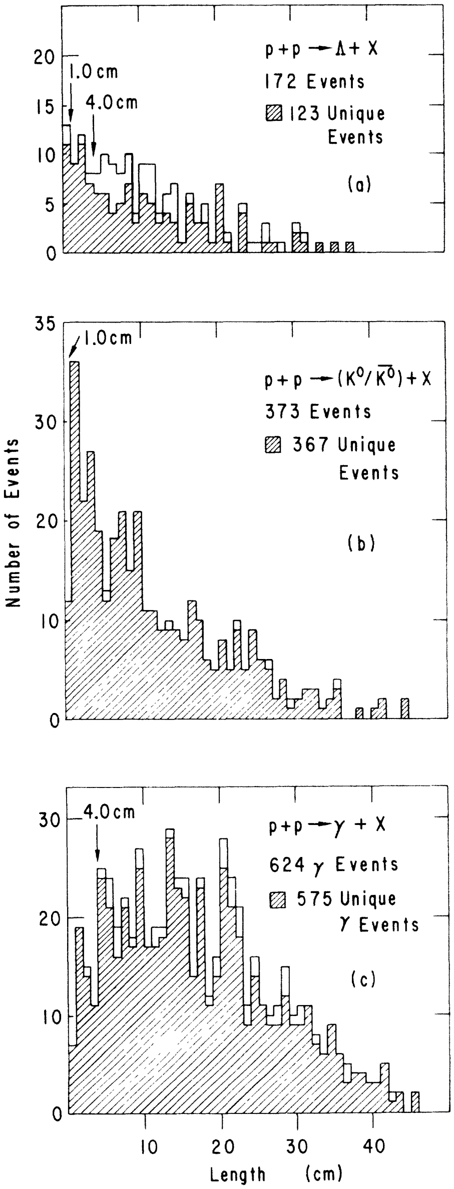

FIG. 2. (a) Length of Λ events from the primary vertex. Events shown are after all ambiguities have been resolved and after fiducial volume cuts. (b) Same as (a) for K^0's. (c) Same as (a) for γ's.

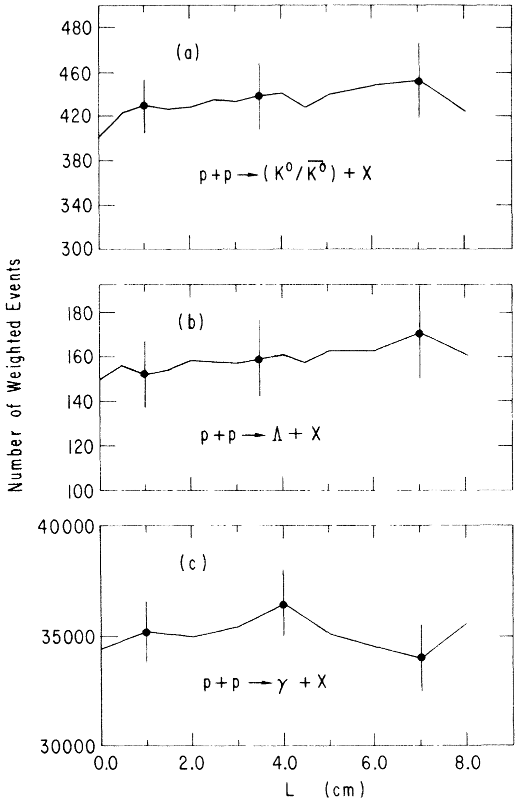

FIG. 3. (a) Weighted number of unique events versus $L_{\min}$ for K^0's with $P_L^* < 0.2$ GeV/c. (b) Same as (a) for unique Λ's with $P_L^* < 0.0$ GeV/c. (c) Same as (a) for all γ's.

cuts of 1.0 cm for Λ and K^0 and 4.0 cm for γ events certainly support such an expectation.

VI. FORWARD-BACKWARD SYMMETRY IN THE OVER-ALL c.m. SYSTEM

Because the initial pp system is symmetric in the overall c.m. the distributions of V^0's and γ's should also be symmetric forward and backward in the c.m. system. However, V^0's produced very forward in the c.m. have high momenta in the lab and so generally leave the chamber before decaying. They also have small opening angles and, in addition, may be obscured by any forward cone of charged tracks from the production vertex, so that the scanning and processing efficiencies for such V^0's are likely to be low. To demonstrate these effects, we show in Figs. 4(a) and 4(b) the weighted P_L^* distributions for the K^0 and Λ sample (P_L^* is the longitudinal momentum in the c.m. system, and can range from -10 to $+10$ GeV/c for 205-GeV/c interactions). The distribution for K's is symmetric out to $P_L^* \simeq 0.4$ GeV/c (corresponding to $P_{\text{lab}} \simeq 11$ GeV/c), but there are clearly losses at larger values of P_L^*. In the rest of the paper, we have kept only K's with $P_L^* < +0.4$ GeV/c, and we have doubled the weights for those with $P_L^* < -0.4$ GeV/c. Λ's in the forward hemisphere have $P_{\text{lab}} \gtrsim 11$ GeV/c and so the few events observed have large weights, causing big fluctuations in the P_L^* distribution and making the forward/backward comparison unreliable. However, we have calculated how many forward Λ's we would expect to see, based on the number of backward hemisphere Λ's that are seen. To do this, each backward Λ in the c.m. system was reflected into the forward hemisphere and then transformed to the lab system. We then calculated the probability of such a Λ decaying within our fiducial volume. The sum of the probability for these Λ's was equivalent to 12 events. This is to be compared with 18 possible Λ fits in the forward hemisphere. However, these fits are highly ambiguous with K^0's and γ's, and we estimate that only 12 to 14 of the candidates are actually Λ's. We have, therefore, retained only the backward Λ's and also doubled the weights for these events.

For γ's, the conversion probability is practically constant for $P_{\text{lab}} > 1$ GeV/c.[4] This means that there should be no bias against detection of forward hemisphere γ's due to escape from the chamber, but there could still be losses due to scanning and processing problems. There is a further complication since for $P_{\text{lab}} < 0.1$ GeV/c, the γ conversion probability falls rapidly to zero and even at $P_{\text{lab}} = 0.1$ GeV/c it is only about half of the asymptotic value at high momenta. The kinematic region for γ's with $P_{\text{lab}} < 0.1$ GeV/c extends from $P_L^* = -2.1$ GeV/c to $P_L^* = +0.005$ GeV/c and out to a transverse momentum $P_\perp$ of 0.1 GeV/c at its maximum. This region is shown on the Peyrou plot for the γ's ($P_\perp$ versus P_L^*) given in Fig. 5, and there is a clear depletion of detected events compared to the corresponding symmetric region in the forward hemisphere. The weighted number of events in the $P_{\text{lab}} < 0.1$ GeV/c regions is 1708 ± 460 (14 ± 4 detected events) compared with 2744 ± 410 for the 45 ± 7 events lying in the reflected region. To

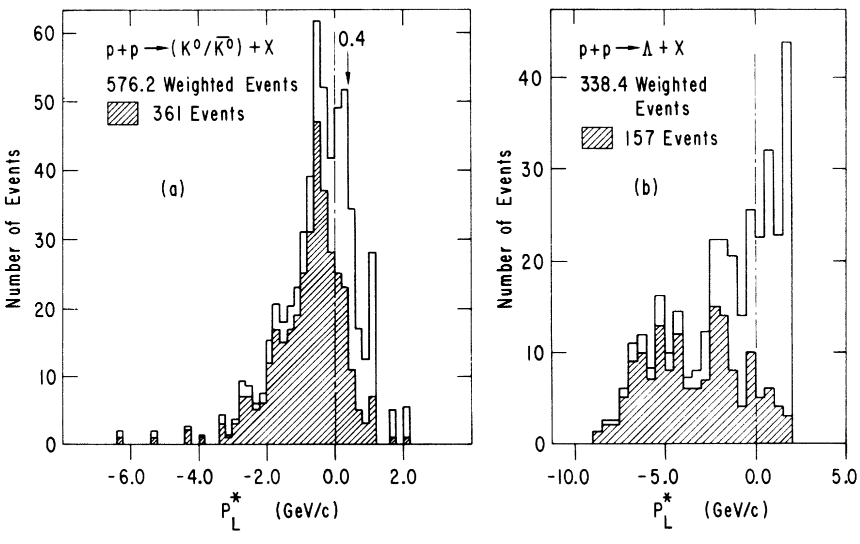

FIG. 4. (a) Histogram of P_L^* for K^0 events after L_{min} and fiducial volume cuts. (b) Same as (a) for Λ's.

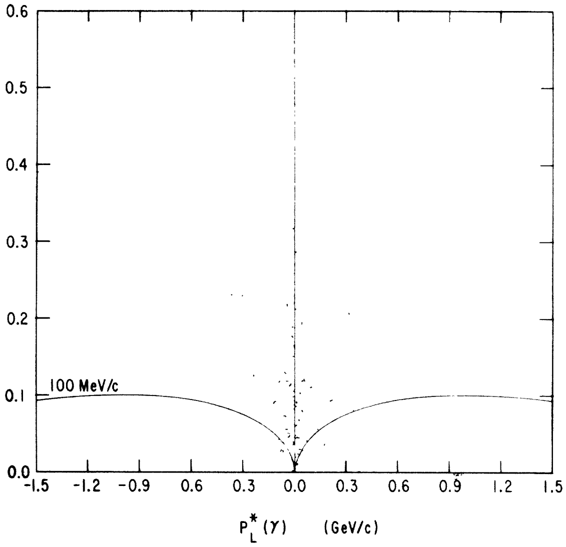

FIG. 5. Peyrou plot ($P_\perp$ vs P_L^*) for γ events. The curve for $P = 100$ MeV/c is shown in the backward hemisphere together with its reflection in the forward hemisphere.

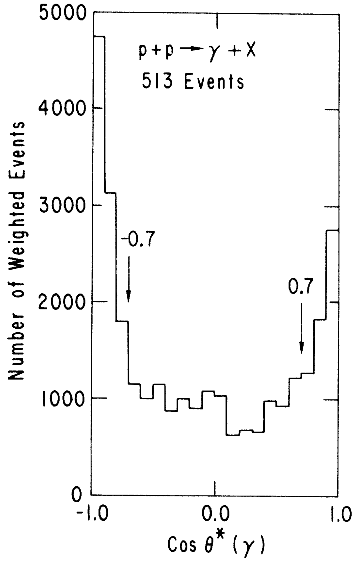

FIG. 6. Distribution of cosθ^* for all selected γ events. Events with $P_{\min} < 100$ MeV/c as well as those that fall under the reflected $P_{\min} = 100$ MeV/c curve have been removed.

check for possible losses of forward hemisphere γ's, events in both of these regions have been excluded and a plot made (Fig. 6) of the distribution in cosθ^*, where θ^* is the c.m. production angle with respect to the incident protons. There is clearly a loss of forward events for cos$\theta^* > 0.70$. This corresponds to 45° in the c.m. system, about 5° in the lab. It is our assumption that these very-forward events are not detected during the scanning stage. The reason is mainly because of the prongs from the primary vertex all lying along the beam direction in a very narrow cone.

The γ events are therefore corrected in two steps. We first remove all events under the $P_{\text{lab}} < 0.1$ GeV/c curve and with $P_L^* \leq 0.0$, and then multiply the weights of the events lying under the reflected curve by 2.0. The second correction then involves the cosθ^*; i.e., we multiply the weight of events in three bins from cos$\theta^* = 0.7$ to 1.0 by the ratio of the weighted event number in the backward to forward bin.

The number of events after all these cuts is given in column 4 of Table III. Column 5 of Table III lists the average weight for the retained events without any symmetry correction. Note, in particular, that the average γ weight is quite large, which is due to the small size of the chamber compared to the γ conversion length in hydrogen.

VII. TOTAL CROSS SECTIONS

Using the selected number of weighted events and correcting for forward/backward losses, we obtain the cross sections. However, several additional corrections must be made. First of all, the unmeasured events (Table I) were added to the appropriate channels in the appropriate topology. Furthermore, scanning efficiencies were folded into weighted event numbers. In addition, Fig. 1(b) indicates that ~7 events are missing in the K^0 sample (i.e., around $P_\perp^{\pi^-} \sim 0.1$ GeV/c). Hence, we assumed that with the previously prescribed selections, seven ambiguous events actually belonging to the K^0 sample were put into the Λ sample. We therefore subtract an appropriate fraction from the Λ events and add an appropriate fraction to the K^0 sample. In addition, the Λ events were corrected for the unseen $\Lambda \rightarrow n\pi^0$ decay mode.[5] For the K^0, we corrected for unseen $K_S^0 \rightarrow \pi^0\pi^0$ decays[5] as well as for missed K_L^0's.

The final cross section values so obtained are

$$\sigma(p+p \rightarrow \Lambda + X) = 3.33 \pm 0.33 \text{ mb},$$

$$\sigma(p+p \rightarrow (K^0/\bar{K}^0) + X) = 11.58 \pm 0.80 \text{ mb},$$

$$\sigma(p+p \rightarrow \gamma + X) = 214.6 \pm 13.7 \text{ mb},$$

$$\sigma(p+p \rightarrow \bar{\Lambda} + X) = 0.40^{+0.14}_{-0.12} \text{ mb}.$$

These values are in good agreement with our earlier data.[1,2] Under the assumption that all γ's originate from $\pi^0 \rightarrow \gamma\gamma$ decays, we then also have

$$\sigma(p+p \rightarrow \pi^0 + X) = 107.3 \pm 6.8 \text{ mb}.$$

The Λ and K^0 cross sections are presented in Figs. 7(a) and 7(b), together with the results from

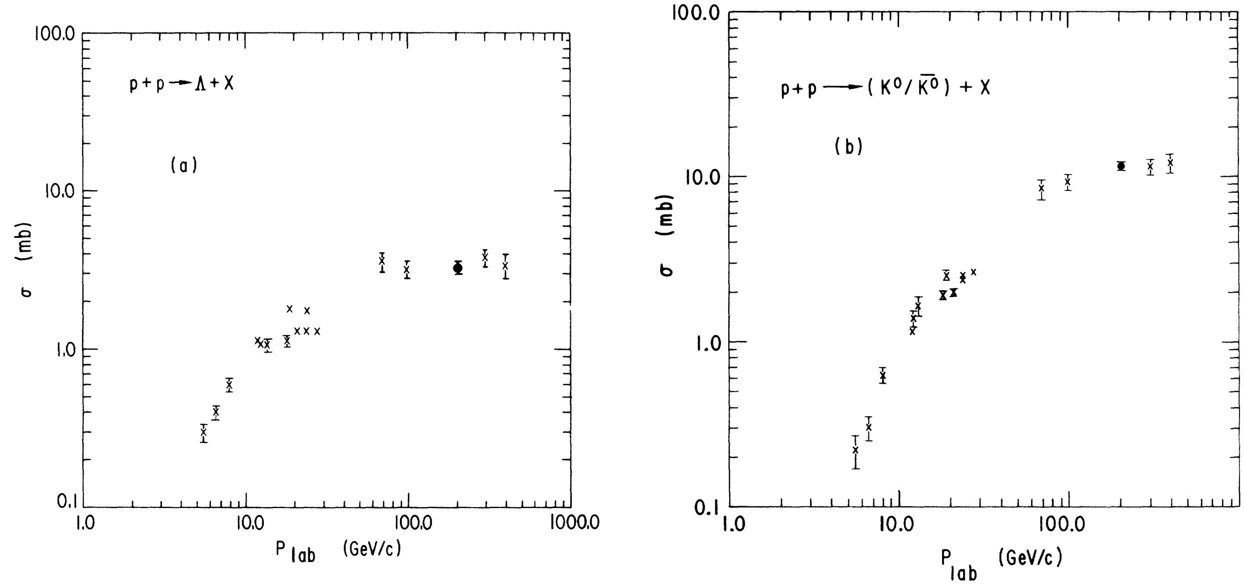

FIG. 7. (a) Total inclusive Λ cross section as a function of P_{lab}. (b) Same as (a) for K^0.

existing world data.[6-14] From the figures, it is evident that both the inclusive Λ as well as the inclusive K^0 cross sections have slowed their rapid increase with increasing momentum in the region of 70–100 GeV/c. A compilation[6-13] of the existing π^0 inclusive cross sections is shown in Fig. 8. The straight line represents an eyeball fit to the predicted π^0 cross section found using the charged-particle data from the compilation of Antinucci *et al.*[15] and the relationship $\sigma(\pi^0) = \frac{1}{2}[\sigma(\pi^+) + \sigma(\pi^-)]$. Evidently, both the measured and the estimated π^0 cross sections rise linearly in ln$s$ up to 400 GeV^2 with the same dependence.

In fig. 9(a) we present the $\gamma\gamma$ mass spectrum of the 2γ events originating from the same primary vertex. No η signal is apparent. Furthermore, by estimating (5 ± 3) π^0 events between $80 < M(\gamma\gamma) < 160$ MeV/c^2, we obtain $\sigma(\pi^0) = 80 \pm 50$ mb, in agreement with the π^0 cross section obtained from the single γ events.

The invariant mass of the $\Lambda\gamma$ events is shown in Fig. 9(b) for those events which have an associated Λ and γ. In the Σ^0 mass region, one can estimate 3 ± 2 events, corresponding to $\sigma(\Sigma^0)$

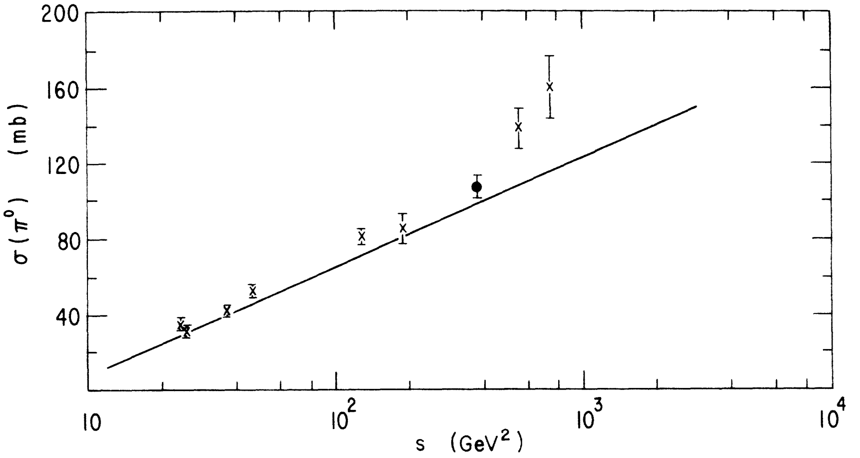

FIG. 8. Total inclusive π^0 cross section as a function of s, the c.m. energy squared. The curve represents an eyeball fit to $\sigma(\pi^0) = \frac{1}{2}[\sigma(\pi^+) + \sigma(\pi^-)]$ data compiled in Ref. 15.

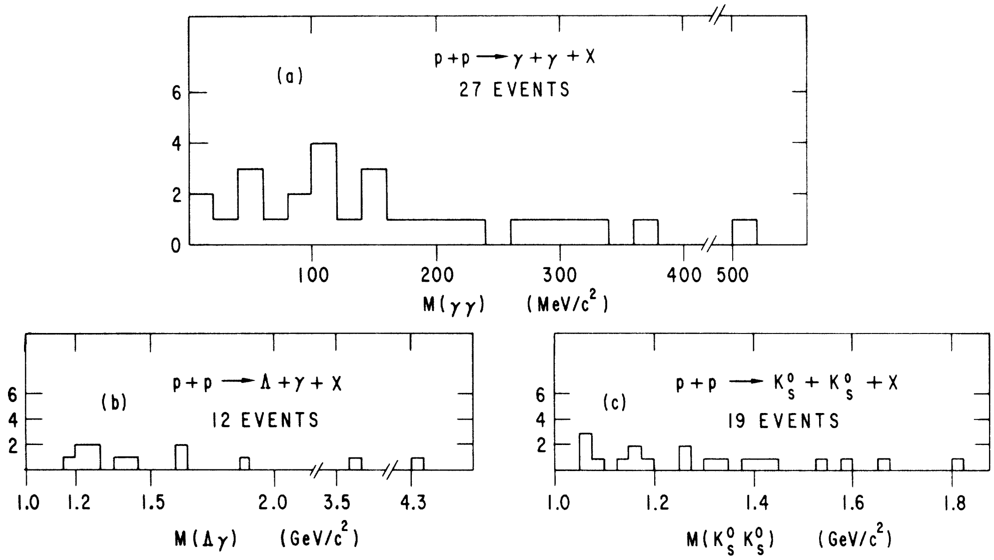

FIG. 9. (a) Invariant mass distribution $M(\gamma\gamma)$ for 2γ events. (b) Invariant mass distribution $M(\Lambda\gamma)$ for Λ plus γ events. (c) Invariant mass distribution $M(K^0_SK^0_S)$ for $2K^0_S$ events.

$\cong 3.32 \pm 2.22$ mb. For completeness, the mass spectrum of $M(K^0_SK^0_S)$ is presented in Fig. 9(c). Clearly no resonance information is evident.

VIII. TOPOLOGICAL CROSS SECTIONS AND MULTIPLICITIES OF THE INCLUSIVE π^0, K^0, Λ EVENTS

The inclusive topological cross sections for $p + p \rightarrow (\gamma, K^0, \Lambda) + X$ production are listed in Table IV. Assuming once again that most of the γ's are from π^0 decays, we then have $\sigma_n(\pi^0) = \frac{1}{2}\sigma_n(\gamma)$, where n stands for the number of charged prongs at the primary vertex. The data is plotted in Figs. 10–10(c) for the Λ, K^0, and π^0 channels, respectively. In all three cases, our values are compared with those from the 12.4- and 69.0-GeV/c experiments.[8,11]

By use of the topological cross sections, we are now able to calculate the average number of $\langle \pi^0 \rangle$, $\langle K^0 \rangle$, and $\langle \Lambda \rangle$ per inelastic collision:

$$\langle V^0 \rangle_n = \sigma_n(V^0)/\sigma_n(pp),$$

TABLE IV. Inclusive topological cross sections for $p + p \rightarrow (\Lambda, K^0, \gamma, \pi^0) + X$.

	Λ events		K^0 events		γ events		
Topology	Raw No. of events	$\sigma(pp \rightarrow \Lambda + X)$ (mb)	Raw No. of events	$\sigma(pp \rightarrow K^0/\bar{K}^0 + X)$ (mb)	Raw No. of events	$\sigma(pp \rightarrow \gamma + X)$ (mb)	$\sigma(pp \rightarrow \pi^0 + X)$ (mb)
2	8	0.193 ± 0.077	10	0.346 ± 0.106	17	7.05 ± 2.02	3.53 ± 1.01
4	25	0.477 ± 0.098	44	1.53 ± 0.25	57	21.6 ± 3.2	10.8 ± 1.59
6	42	0.892 ± 0.145	77	2.67 ± 0.30	105	43.5 ± 5.1	21.8 ± 2.6
8	21	0.422 ± 0.096	60	2.11 ± 0.29	108	38.4 ± 4.5	19.2 ± 2.3
10	23	0.732 ± 0.166	68	2.31 ± 0.29	118	45.8 ± 4.7	22.9 ± 2.4
12	10	0.307 ± 0.090	37	1.28 ± 0.21	70	24.8 ± 3.3	12.4 ± 1.7
14	4	0.115 ± 0.063	14	0.451 ± 0.122	44	17.7 ± 2.9	8.83 ± 1.47
16	2	0.041 ± 0.027	12	0.506 ± 0.139	23	10.3 ± 2.2	5.17 ± 1.09
18	4	0.145 ± 0.073	8	0.279 ± 0.098	8	2.35 ± 0.85	1.18 ± 0.43
20	···	···	···	···	3	0.781 ± 0.470	0.390 ± 0.232
22	···	···	1	0.045 ± 0.045	3	0.940 ± 0.629	0.470 ± 0.315
24	···	···	2	0.050 ± 0.036	···	···	···
26	···	···	···	···	2	1.47 ± 1.18	0.735 ± 0.590
Total	139	3.33 ± 0.33	333	11.58 ± 0.80	558	214.6 ± 13.7	107.3 ± 6.8

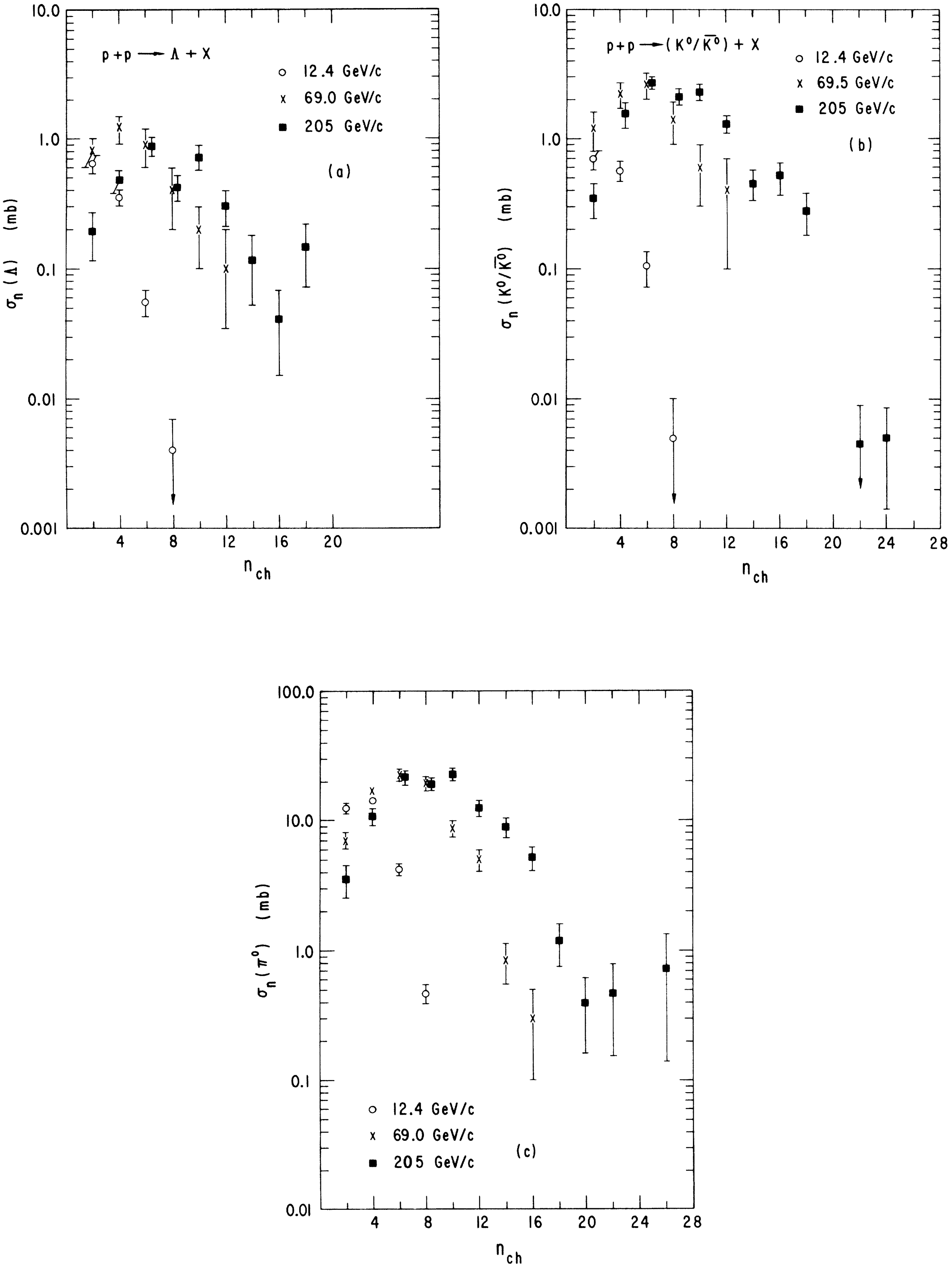

FIG. 10. (a) Topological cross sections for inclusive Λ events at 12.4, 69.0, and 205 GeV/c. (b) Same as (a) for inclusive K^0 events. (c) Same as (a) for inclusive π^0 events.

where V^0 stands for π^0, K^0, or Λ. The inelastic topological pp cross sections for this experiment are given in Table V,[16] together with the average values.

Figure 11(a) shows our values for the inclusive Λ's. Because of the limited statistics, no conclusion as to the shape of this distribution can be drawn at this time. In fact, the data are consistent with being flat.

The $\langle K^0/\bar{K}^0\rangle$ values are shown in Fig. 11(b). In this case, a linear rise is evident up to $n_{\text{ch}}=10$. The broken line in the figure corresponds to a fit for $\langle K^0/\bar{K}^0\rangle = \alpha + \beta\, n_{\text{ch}}$, with $\alpha = 0.05 \pm 0.05$ and $\beta = 0.046 \pm 0.008$.[17] In addition, it should be noted that the shape of the distribution up to $n_{\text{ch}} = 14$ agrees with the critical-point theory as presented by Thomas.[18]

The linear rise of $\langle \pi^0\rangle$ versus n_{ch} is apparent for events with 2 to 16 prongs as shown in Fig. 11(c). The broken curve represents a linear fit with $\alpha = 0.61 \pm 0.32$ and slope $\beta = 0.35 \pm 0.05$.[19] The solid line on the graph represents a prediction of the critical-point model[18] which appears to agree quite well with the experiment. Using this model, one can also estimate the number of seen 2γ events using our overall single-γ detection efficiency of 0.01245. The model predicts 30 two-γ events compared to 27 found, which once again is in good agreement.

Finally, it is amusing to note that Fig. 11 gives a hint of an odd-even effect in $\langle \pi^0\rangle$ versus n_- with the correlation larger when there is an even number of π^-. Arneodo and Kubar-Andre[20] have given an example of a theoretical model which produces odd-even correlation effects between π^0 and π^-. Their model allows for production of ρ mesons in paris which increase the likelihood of observing a π^0 when there is an odd number of π^- present. Apparently, their model is then just out of phase with the possible trend hinted at in Fig. 11.

IX. DIFFERENTIAL CROSS SECTIONS

In order to discuss the energy dependence of the Λ, K^0, and π^0 inclusive spectra, we use the invariant cross section

$$F(x, P_\perp, s) = \frac{2E^*}{\pi\sqrt{s}}\,\frac{d^2\sigma}{dx\,dP_\perp^{\,2}}\,, \tag{8}$$

with E^* being the energy of the particle in the overall c.m. system, $P_\perp$ being the transverse momentum of the particle, s being the square of the total center-of-mass energy, x being the Feynman variable defined as $x = 2P_L^*/\sqrt{s}$, and P_L^* being the longitudinal momentum of the particle in the overall c.m. system. Because of the limited statistics involved in this experiment, we have folded the forward and backward events with respect to $x = 0$ and added the distributions. Figures 12(a)–12(c) display the differential cross sections $d\sigma/d|x|$ for the inclusive Λ, K^0, and γ data. In all three cases, the data are compared with those obtained at 12.4 GeV/c.[8] We note in Fig. 12(a) that the increase in total cross section from 1.07 to 3.33 mb is due to increased Λ production throughout the $|x|$ region up to 0.8. This can be contrasted to Fig. 12(b), which shows that the

TABLE V. Average number of Λ, K^0, and π^0 per inelastic collision.

Topology	$\sigma_n\,(pp)$ (mb)	$\langle\Lambda\rangle$	$\langle K^0/\bar{K}^0\rangle$	$\langle\pi^0\rangle$
2	2.85 ± 0.26	0.068 ± 0.028	0.121 ± 0.039	1.24 ± 0.37
4	5.91 ± 0.28	0.081 ± 0.017	0.259 ± 0.044	1.83 ± 0.28
6	6.89 ± 0.32	0.130 ± 0.022	0.388 ± 0.047	3.16 ± 0.40
8	5.73 ± 0.28	0.074 ± 0.017	0.368 ± 0.054	3.35 ± 0.43
10	4.56 ± 0.24	0.161 ± 0.037	0.507 ± 0.069	5.02 ± 0.58
12	3.23 ± 0.18	0.095 ± 0.028	0.396 ± 0.069	3.84 ± 0.56
14	1.58 ± 0.11	0.098 ± 0.054	0.285 ± 0.080	5.59 ± 1.01
16	0.846 ± 0.075	0.049 ± 0.033	0.598 ± 0.173	6.11 ± 1.40
18	0.335 ± 0.044	0.432 ± 0.225	0.833 ± 0.312	3.52 ± 1.36
20	0.121 ± 0.025	···	···	3.23 ± 2.03
22	0.053 ± 0.016	···	0.849 ± 0.849	8.87 ± 6.52
24	0.012 ± 0.008	···	4.17 ± 4.09	···
26	0.004 ± 0.004	···	···	17.8 ± 17.8
Total	32.1 ± 1.1	0.103 ± 0.011	0.361 ± 0.028	3.34 ± 0.24

increase in the total cross section from 1.37 to 11.58 mb is primarily due to K^0 production in the central region $|x| \leq 0.4$.

The data for the inclusive γ production [Fig. 12(c)] looks quite different from the K^0 and Λ samples. Once again, as in the K^0 case, the increase of the total inclusive cross section from 61.1 mb at 12.4 GeV/c to 214.6 mb at 205 GeV/c is primarily due to γ production throughout the $|x|$ region (0.0 → 0.4). The solid line in Fig. 12(c) represents data from the π^- and π^+ events from this experiment. Explicitly, it is the sum of $\frac{1}{2}[d\sigma/d|x|(\pi^- \to \gamma\gamma) + d\sigma/d|x|(\pi^+ \to \gamma\gamma)]$. In order to obtain this curve, we have taken measured positive and negative tracks and removed the bulk of protons. The remaining tracks were then assumed to be π^+'s or π^-'s and were allowed to decay into $\gamma\gamma$ via a Monte Carlo technique. The resulting γ distributions were normalized to the total inclusive π^+ and π^- cross sections. The goodness of fit of the curve in Fig. 12(c) to the data is a measure of how well the relationship $d\sigma/dx(\pi^0) = \frac{1}{2}[d\sigma/dx(\pi^+) + d\sigma/dx(\pi^-)]$ (and simple kinematics) describes the data. The agreement is seen to be excellent.[21]

By integrating Eq. (8) over $P_\perp^2$, we obtain

$$F_1(x,s) = \int \frac{2E^*}{\pi\sqrt{s}} \frac{d^2\sigma}{dx\,dP_\perp^2}\, dP_\perp^2 . \qquad (9)$$

If Feynman scaling exists, then this function will become independent of s. In Figs. 13(a)–13(c) we show this function versus $|x|$ for this experiment and for data from the 12.4- (Ref. 8) and 69.0- (Ref. 11) GeV/c experiments. All the Λ, K^0, and γ data indicate that within the experimental errors, scaling has set in below 69 GeV/c.

The differential cross sections $d\sigma/dP_\perp^2$ for inclusive Λ, K^0, γ production are shown in Figs. 14(a)–14(c), respectively. In all three cases, a comparison with the data at 12.4 GeV/c (Ref. 8) is presented. The distributions for K^0 and γ look very similar at the two energies 12.4 and 205 and GeV/c. The Λ data [Fig. 14(a)] at 205 GeV/c shows evidence for a break-in slope at $P_\perp^2 \simeq 0.3$ (GeV/c)^2. The curve in Fig. 14(c) represents data from the π^+ and π^- tracks as outlined above. Once again, the agreement between the measured $d\sigma/dP_\perp^2(\gamma)$ and the curve is excellent, suggesting once again that $d\sigma/dP_\perp^2(\pi^0) = \frac{1}{2}[d\sigma/dP_\perp^2(\pi^+) + d\sigma/dP_\perp^2(\pi^-)]$ throughout the $P_\perp^2$ range at this energy. Hence, we have now shown that at this energy not only $\sigma(\pi^0) = \frac{1}{2}[\sigma(\pi^+) + \sigma(\pi^-)]$ holds (see Fig. 8), but also that the differential cross section agrees with this relationship.

The rapidity distributions in the over-all c.m. system are presented in Fig. 15(a) for Λ and K^0 and in Fig. 15(b) for γ production. The rapidity y^* is defined by

$$y^* = \tfrac{1}{2}\ln\left(\frac{E^* + P_L^*}{E^* - P_L^*}\right), \qquad (10)$$

with all asterisked quantities referring to the c.m. system. The K^0 distribution shows a dip in the central region near $y^* = 0$, whereas the Λ spectrum indicates larger cross section around $|y^*| = 2.0$. The γ data is compared with that from the 12.4-GeV/c experiment[8] and indicates an increase of the central plateau from 1.5 to 3.0 units of rapidity.

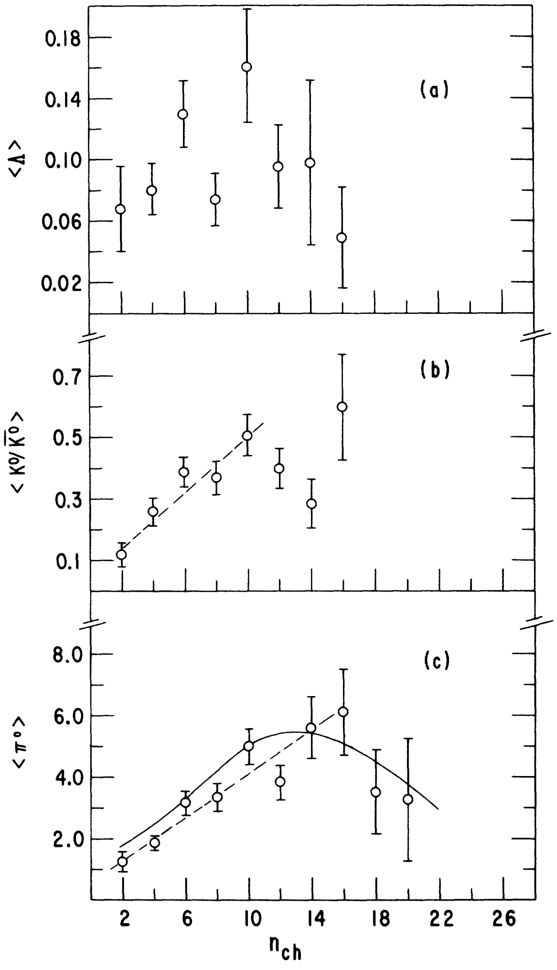

FIG. 11. (a) Average values $\langle\Lambda\rangle$ as a function of topology. (b) Same as (a) for $\langle K^0/\bar{K}^0\rangle$. The straight line corresponds to a linear fit of slope 0.046± 0.008 for values at 2 to 10 prongs. (c) Same as (a) for $\langle\pi^0\rangle$. The solid curve represents a prediction of the critical-point model. The broken line corresponds to a linear fit of slope 0.35± 0.05 for values at 2 to 16 prongs.

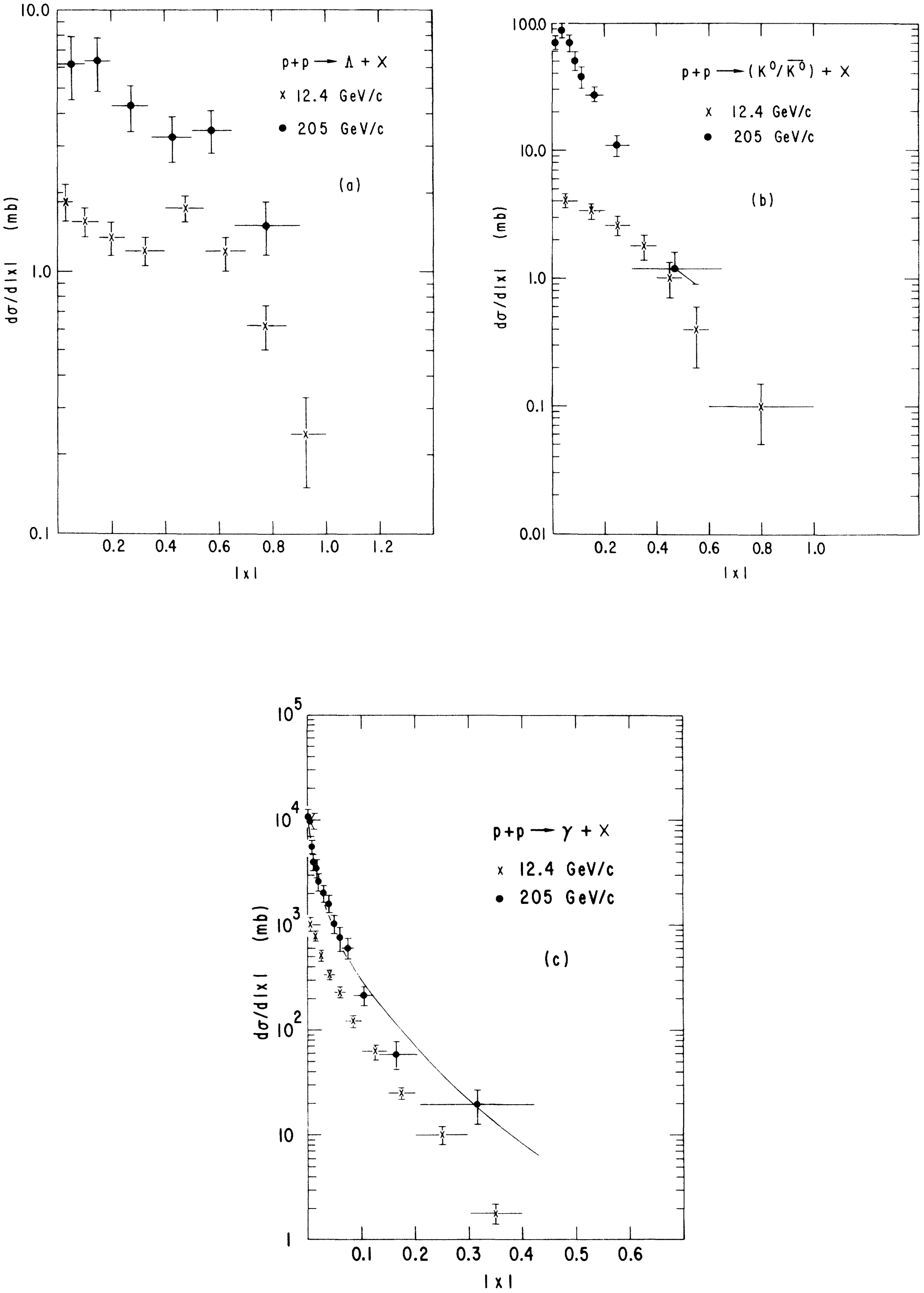

FIG. 12. (a) Differential cross sections $d\sigma/d|x|$ for inclusive Λ events. The data has been folded about $x=0$ and added. Data points are presented for this experiment and for data at 12.4 GeV/c. (b) Same as (a) for inclusive K^0 production. (c) Same as (a) for inclusive γ production. The solid line represents data from this exposure for $\frac{1}{2}[d\sigma/d|x|(\pi^+ \rightarrow \gamma\gamma) + d\sigma/d|x|(\pi^- \rightarrow \gamma\gamma)]$ in which the charged π's were allowed to decay by a Monte Carlo technique into two γ's (see text for further details).

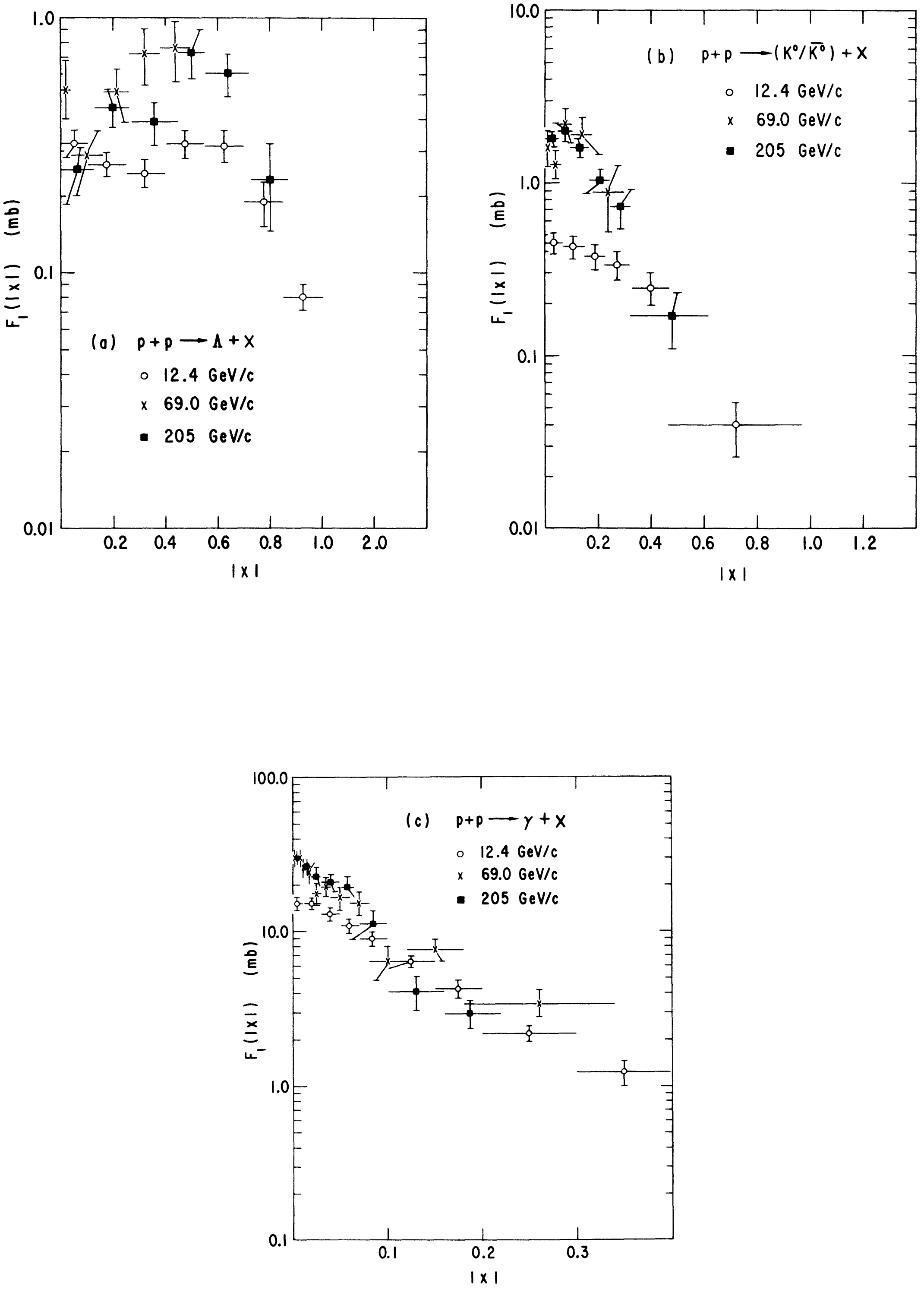

FIG. 13. (a) $F_1(|x|)$ for inclusive Λ events at 12.4, 69.0, and 205 GeV/*c*. (b) Same as (a) for inclusive $K^0/\bar{K}^0$ events. (c) Same as (a) for inclusive γ events.

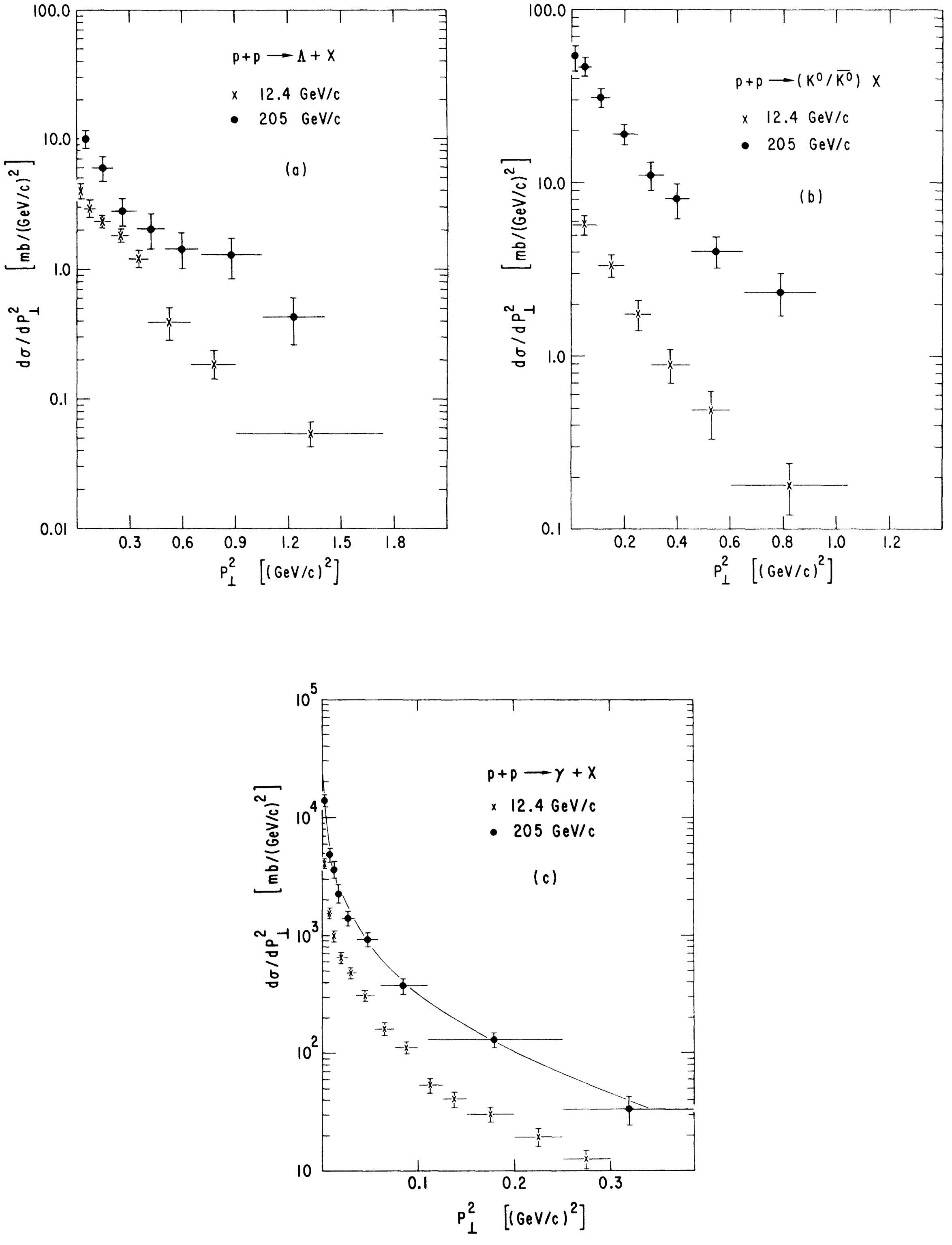

FIG. 14. (a) Differential cross sections $d\sigma/dP_\perp^2$ for inclusive Λ events at 12.4 and 205 GeV/c. (b) Same as (a) for inclusive $K^0/\bar{K}^0$. (c) Same as (a) for inclusive γ's. The solid line represents data from this exposure for $\frac{1}{2}[d\sigma/dP_\perp^2(\pi^+ \rightarrow \gamma\gamma) + d\sigma/dP_\perp^2(\pi^- \rightarrow \gamma\gamma)]$ in which the charged π's were allowed to decay by a Monte Carlo technique into two γ's (see text for further details).

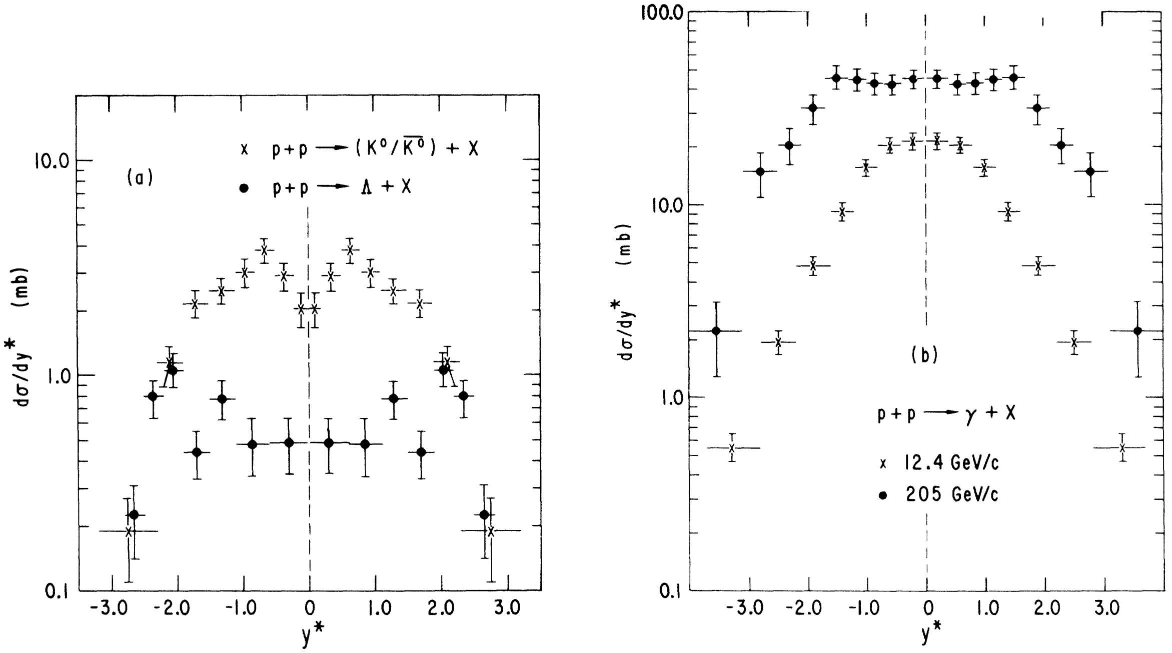

FIG. 15. (a) Differential cross sections as a function of rapidity in the overall c.m. system for inclusive $K^0/\bar{K}^0$ and Λ events. (b) Same as (a) for γ events at 12.4 and 205 GeV/c.

X. ASSOCIATED CHARGED MULTIPLICITIES

Results of the calculations for the charged multiplicities associated with the production of γ, K^0, or Λ as a function of the corresponding $|x|$ are presented in Fig. 16. The Λ [Fig. 16(a)] and K^0 [Fig. 16(b)] data are compared with those results from the 12.4-(Ref. 8) and 19-GeV/c-(Ref. 22) experiments. In both cases, a decrease of $\langle n_{ch}\rangle$ with increasing $|x|$ is evident at all energies. Furthermore, the graphs clearly indicate the over-all increase of $\langle n_{ch}\rangle$ with increasing energy. The inclusive γ data is presented in Fig. 16(c) together with π^- points from the 19-GeV/c experiment.[22] Once again a slow falloff of $\langle n_{ch}\rangle$ with increasing $|x|$ is evident. When plotted as a function of $P_\perp$, the values of the associated charged multiplicities for K^0 and γ tend to stay constant. In the case of Λ production at 205 GeV/c, the associated charged multiplicities may be slowly increasing with $P_\perp$. This is demonstrated in Figs. 17(a)–17(c) for the Λ, K^0, γ data, respectively. The Λ and K^0 data once again are compared with data at 12.4 (Ref 8) and 19 (Ref. 22) GeV/c and they show an increase of $\langle n_{ch}\rangle$ with energy throughout the $P_\perp$ range. The γ data [Fig. 17(c)] are compared with the π^- points obtained from the 19-GeV/c experiment.[22] It should also be noted that for this experiment, the associated charged multiplicities for γ, K^0, Λ production indicate common $|x|$ dependence in the overlapping regions. The same appears to be true in terms of $P_\perp$ for K^0 and γ events, but not for the Λ's.

The missing mass recoiling off the γ, K^0 or Λ of reactions (1), (2), and (3) are graphed in differential form in Fig. 18(a). Besides the different thresholds associated with these reactions, we observe smooth distributions for the γ, K^0, and Λ events. Results of the calculations of the associated charged multiplicities as a function of $(\mathrm{MM})^2$ are presented in Fig. 18(b). Once again, the values indicate common $(\mathrm{MM})^2$ dependence in the overlapping regions.

XI. AVERAGE VALUES AND f_2^{00}

Average values were determined for $P_\perp$, $P_\perp^2$, $|P_L^*|$, and P_L^{*2} for the γ, K^0, and Λ events. The results are listed in Table VI. By use of $\langle P_\perp^2\rangle_{\pi^0} = 3\langle P_\perp^2\rangle_\gamma - \frac{1}{2}M_{\pi^0}^2$, $\langle P_L^*\rangle_{\pi^0} = 2\langle P_L^*\rangle_\gamma$, $\langle P_L^{*2}\rangle_{\pi^0} = 3\langle P_L^{*2}\rangle_\gamma - \frac{1}{4}M_{\pi^0}^2$,[23] we are also able to determine some values for π^0 assuming that all γ's originated from π^0 decays. By comparing the $\langle P_\perp\rangle$ values with those obtained at 12.4 GeV/c,[8] namely $\langle P_\perp\rangle_\Lambda = 0.467 \pm 0.013$, $\langle P_\perp\rangle_{K^0} = 0.415 \pm 0.016$, $\langle P_\perp\rangle_\gamma = 0.155 \pm 0.012$, we observe that $\langle P_\perp\rangle$ has not changed between 12.4 and 205 GeV/c for Λ and K^0 production. In the case of γ's, $\langle P_\perp\rangle$ increases by 30% from 0.155 to 0.199.

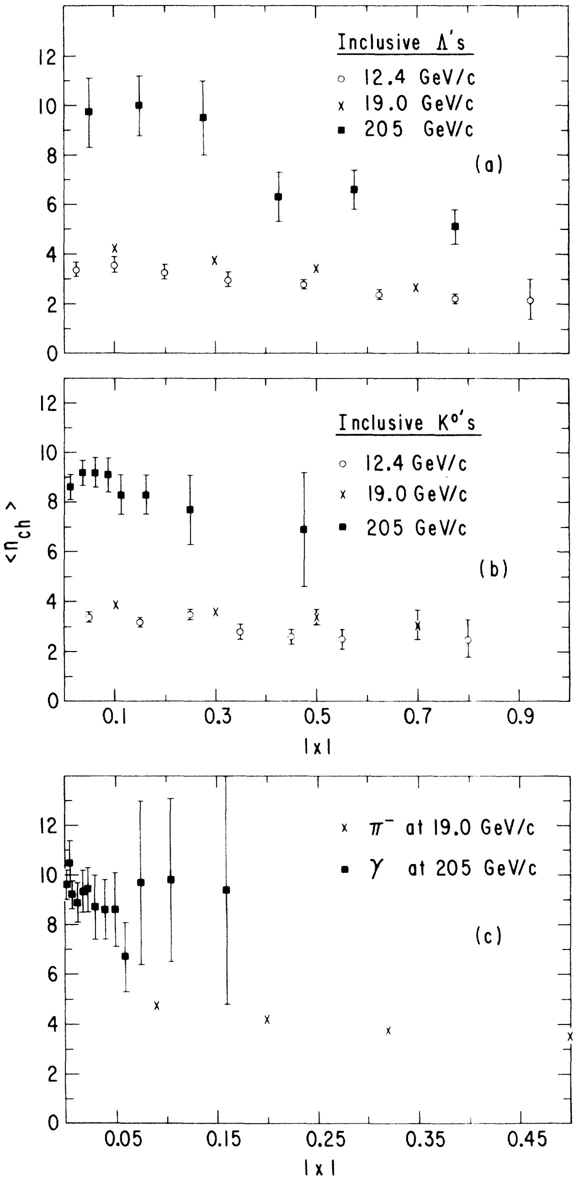

FIG. 16. (a) Associated charged multiplicities as a function of $|x|$ for inclusive Λ events at 12.4, 19.0, and 205 GeV/c. (b) Same as (a) for $K^0/\bar{K}^0$ events. (c) Same as (a) for π^- at 19.0 GeV/c and for γ at 205 GeV/c.

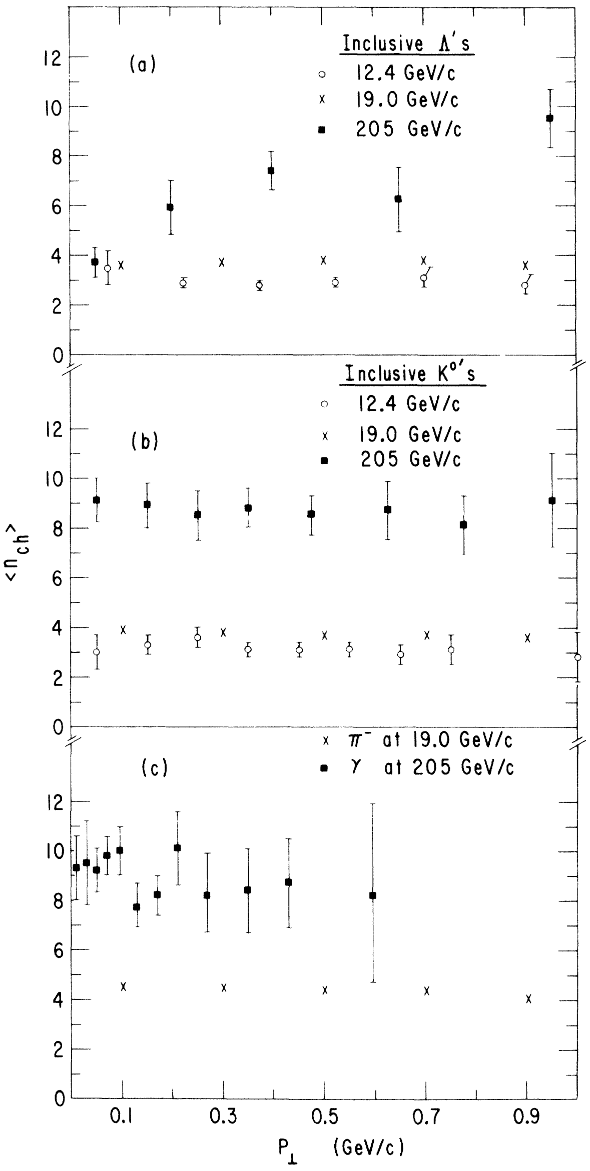

FIG. 17. (a) Associated charged multiplicities as a function of $P_\perp$ for inclusive Λ events at 12.4, 19.0, and 205 GeV/c. (b) Same as (a) for $K^0/\bar{K}^0$. (c) Same as (a) for π^- at 19.0 GeV/c and γ at 205 GeV/c.

The Mueller correlation parameter for $\pi^0\pi^0$ production can be determined from

$$f_2^{00} = \langle n_0(n_0 - 1)\rangle - \langle n_0\rangle^2 ,$$

where n_0 is the number of π^0's produced. Assuming once again that most γ's originate from π^0 decays, this expression can be rewritten as

$$f_2^{00} = \tfrac{1}{4}[\langle n(n-1)\rangle - \langle n\rangle^2] - \tfrac{1}{4}\langle n\rangle ,$$

where n stands for the number of γ's. Unfortunately, this experiment has limited statistics. Nevertheless, f_2^{00} was determined as $-(0.2 \pm 2.9)$ using the 506 single- and 26 double-γ events.

XII. MOMENTUM TRANSFER DISTRIBUTION AND POLARIZATION OF THE Λ

A. Momentum transfer distributions

The momentum transfer distribution $|t - t_{\min}| = t'$ between the Λ and proton is plotted in Fig.

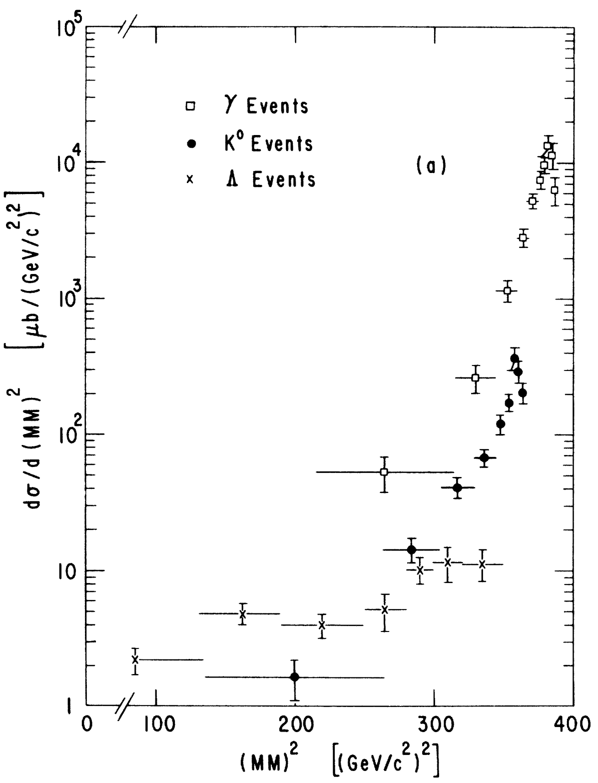

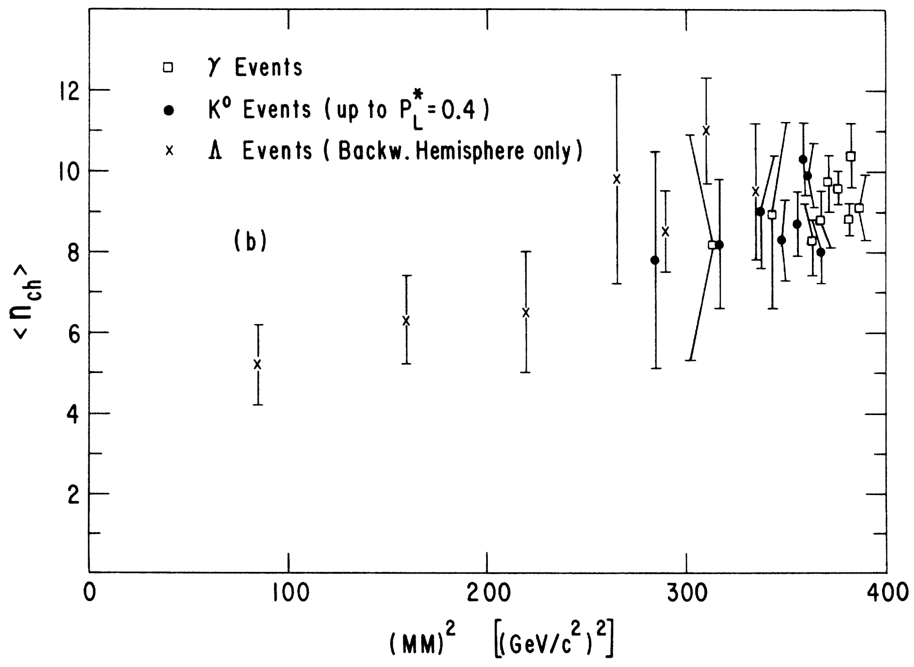

FIG. 18. (a) Differential cross sections as a function of $(\mathrm{MM})^2$, the missing mass squared recoiling off the Λ's, K^0's, or γ's. (b) Associated charged multiplicities as a function of $(\mathrm{MM})^2$ for Λ, K^0, and γ events.

TABLE VI. Average values for γ, π^0, K^0, Λ events.

	$\langle P_\perp \rangle$ (GeV/c)	$\langle P_\perp^2 \rangle$ [(GeV/c)^2]	$\langle \lvert P_L^* \rvert \rangle$ (GeV/c)	$\langle P_L^{*2} \rangle$ [(GeV/c)^2]
γ	0.199 ± 0.008	0.078 ± 0.001	0.317 ± 0.021	0.345 ± 0.061
π^0	...	0.224 ± 0.003	0.634 ± 0.042	1.03 ± 0.18
$K^0/\bar{K}^0$	0.412 ± 0.014	0.234 ± 0.019	1.07 ± 0.05[a]	1.98 ± 0.23[a]
Λ	0.504 ± 0.026	0.345 ± 0.033	3.84 ± 0.19[a]	19.6 ± 1.5[a]

[a] Only events from the backward hemisphere were employed.

19(a). A very sharp break is evident at $|t'| = 1.5$ (GeV/c)^2. The differential distribution was fitted with an exponential of the form

$$\frac{d\sigma}{d|t'|} = A e^{B|t'|} .$$

This fit yielded

$$A = 3.76 \pm 0.95 \text{ mb/(GeV/}c)^2 ,$$

$$B = -(1.60 \pm 0.28) \text{ (GeV/}c)^{-2}$$

for $0.0 \leq |t'| < 1.5$ (GeV/c)^2, and

$$A = 0.40 \pm 0.18 \text{ mb/(GeV/}c)^2 ,$$

$$B = -(0.20 \pm 0.08) \text{ (GeV/}c)^{-2}$$

for $1.5 < |t'| < 10.0$ (GeV/c)^2. By comparing the fits with those obtained at 12.4 GeV/c,[8] we not only find identical slopes for small $|t'|$, but also the occurrence of the break in the distribution at the same $|t'|$ value. The slopes for higher values of $|t'|$ differ by a factor of 3.5 between the two energies.

Distributions for the K^0 events are presented in Fig. 19(b). Once again, a break is evident at this energy. By fitting the data with the above exponential dependence, we obtained

$$A = 6.86 \pm 1.83 \text{ mb/(GeV/}c)^2 ,$$

$$B = -(1.61 \pm 0.76) \text{ (GeV/}c)^{-2}$$

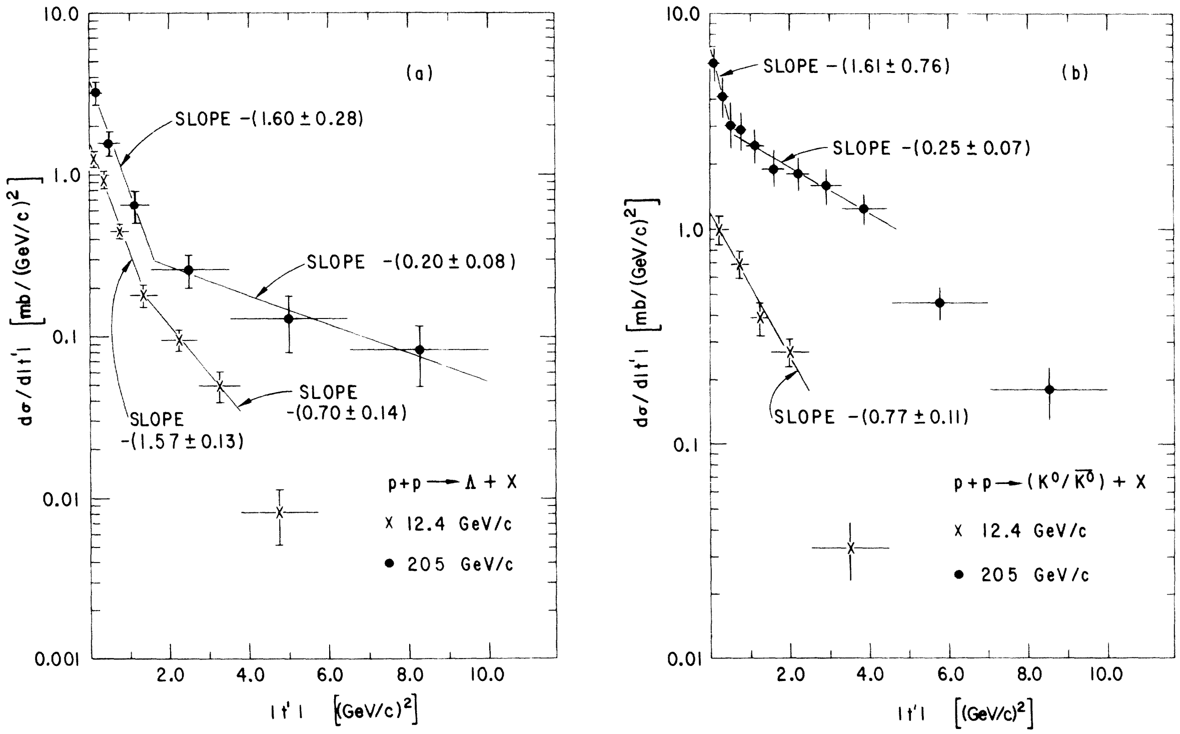

FIG. 19. (a) Momentum transfer distribution for inclusive Λ events at 12.4 and 205 GeV/c. (b) Same as (a) for $K^0/\bar{K}^0$.

for $0.0 \leq |t'| < 0.5$ $(\mathrm{GeV}/c)^2$ and

$$A = 3.18 \pm 1.63\ \mathrm{mb}/(\mathrm{GeV}/c)^2,$$

$$B = -(0.25 \pm 0.07)\ (\mathrm{GeV}/c)^{-2}$$

for $0.5 < |t'| < 4.5$ $(\mathrm{GeV}/c)^2$. By comparison, the data from the 12.4-GeV/c experiment[8] indicates only one slope [Fig. 19(b)]. However, the latter data lack sufficient statistics as is evident from the $|t'|$ range of the first bin, which, for the 205-GeV/c K^{0}'s, is divided into three.

By comparing the Λ and K^0 slopes from the 205-GeV/c data only, we find them to be almost identical. The only difference appears to be the location of the break, located at $|t'| = 0.5$ $(\mathrm{GeV}/c)^2$ for K^{0}'s versus 1.5 $(\mathrm{GeV}/c)^2$ for Λ's.

B. Polarization of the Λ

By use of $W(\cos\theta) = \frac{1}{2}(1 + \alpha P \cos\theta)$, we have calculated the Λ polarization where P = polarization and $\alpha = 0.647$.[5] Defining n = normal to the production plane,

$$n = \vec{P}_B \times \vec{\Lambda} / |\vec{P}_B \times \vec{\Lambda}|\ ,$$

with $\vec{P}_B$, and $\vec{\Lambda}$ being the beam proton and Λ laboratory momenta, respectively, we calculated $\cos\theta = \hat{n} \cdot \hat{p}$, with $\hat{p}$ = momentum of the proton from the Λ decay in the Λ rest frame. Using the above distribution function, we obtain

$$P = \frac{3}{\alpha} \langle \cos\theta \rangle$$

$$= -(0.25 \pm 0.26)$$

for all events. In Fig. 20, we have plotted the polarization as a function of $|x|$. It is clear that the total value as well as all values in Fig. 20 are consistent with zero.

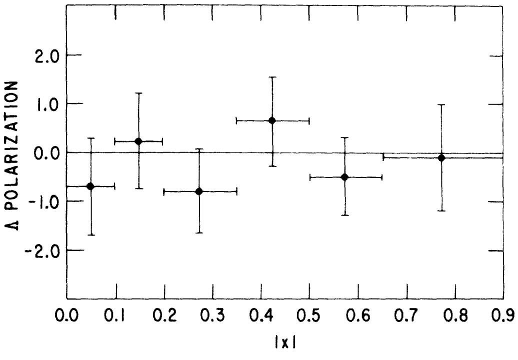

FIG. 20. Polarization of Λ events as a function of $|x|$.

XIII. CONCLUSION

We have presented experimental results on inclusive γ, π^0, $K^0/\bar{K}^0$, and Λ production in pp interactions at 205 GeV/c. The main results are the following:

(a) The average numbers of π^0 agree well with the critical-point model when plotted as a function of topology. The same holds true for the average number of $K^0/\bar{K}^0$. In both cases, the data is also consistent with a linear relationship. For $\langle \pi^0 \rangle$ the slope is 0.35 ± 0.05 from 2 to 16 prongs, whereas for $\langle K^0/\bar{K}^0 \rangle$ the slope is 0.046 ± 0.008 from 2 to 10 prongs.

(b) Comparison of the measured γ distributions with Monte Carlo generated $\pi^- \rightarrow \gamma\gamma$ and $\pi^+ \rightarrow \gamma\gamma$ distributions indicate that $d\sigma/dP_u(\pi^0) = \frac{1}{2}[d\sigma/dP_u(\pi^+) + d\sigma/dP_u(\pi^-)]$ for all values of P_u ($P_u = P_L^*$ or $P_\perp$). Invariant cross sections for γ, K^0, and Λ production indicate that scaling has set in below 69 GeV/c.

(c) The rapidity distributions in the over-all c.m. system indicate a plateau with a full width of 3.0 units for γ events. A dip is observed in the central region for K^0 production.

(d) The charged multiplicities associated with γ and K^0 production tend to stay constant when plotted as a function of $P_\perp$. In the case of Λ production, these values appear to be slowly increasing with $P_\perp$.

(e) The differential cross sections $d\sigma/dt'$ indicate a break at $t' = 1.5$ and 0.5 $(\mathrm{GeV}/c)^2$ for Λ and K^0 production, respectively.

(f) Values for Λ polarization as a function of x are all consistent with zero.

ACKNOWLEDGMENTS

We thank the 30-in. bubble chamber personnel for their work in obtaining the pictures. The careful work by the scanning and measuring personnel is greatly appreciated. The encouragement and support by M. Derrick, T. Fields, and B. Musgrave are greatly appreciated.

---

*On leave of absence from Birmingham University, Birmingham, England.

†Work supported by the U. S. Atomic Energy Commission.

[1] G. Charlton *et al.*, Phys. Rev. Lett. 29, 1759 (1972).

[2] G. Charlton *et al.*, Phys. Rev. Lett. 30, 574 (1973).

[3] We have performed an extensive study of the ambiguous Λ/K^0 events. In particular, all physics distributions

in both channels were checked by leaving all ambiguous events in one or the other channel or by removing them altogether. We conclude from these studies, at this present statistical level, that our distributions are not sensitive to possible event misidentification.

[4] T. M. Knasel, DESY Reports Nos. 70/2 and 70/3, 1970 (unpublished).

[5] Particle Data Group, Phys. Lett. 50B, 1 (1974).

[6] Data points at 5.45 and 6.60 GeV/c are from A. B. Wicklund, Argonne National Laboratory (private communications). Data points at 8.0 GeV/c are from M. W. Firebaugh, Ph.D. thesis, Univ. of Illinois, 1966 (unpublished), and M. W. Firebaugh *et al.*, Phys. Rev. 172, 1354 (1968).

[7] V. Blobel *et al.*, Nucl. Phys. B69, 454 (1974). Beam momenta are at 12.0 and 24.0 GeV/c.

[8] K. Jaeger *et al.*, Phys. Rev. D 11, 1756 (1975). Beam momentum at 12.4 GeV/c.

[9] H. Bøggild *et al.*, Nucl. Phys. B57, 77 (1973); *ibid.* B27, 285 (1971). Beam momentum at 19 GeV/c.

[10] B. Y. Oh and G. A. Smith, Nucl. Phys. B49, 14 (1972). Beam momenta at 13.0, 18.0, 21.0, 24.0, and 28.0 GeV/c.

[11] H. Blumenfeld *et al.*, Phys. Lett. 45B, 525 (1973); *ibid.* 45B, 528 (1973). Beam momentum at 69 GeV/c.

[12] J. W. Chapman *et al.*, Phys. Lett. 47B, 465 (1973). Beam momentum at 102 GeV/c.

[13] F. T. Dao *et al.*, Phys. Rev. Lett. 30, 1151 (1973). Updated at the Meeting of the American Physical Society, Washington, D.C., 1974. Beam momentum at 303 GeV/c.

[14] A. A. Seidl *et al.*, report given at the Meeting of the American Physical Society, Washington, D.C., 1974 (unpublished). See also Ref. 12. Beam momentum at 405 GeV/c.

[15] M. Antinucci *et al.*, Nuovo Cimento Lett. 6, 121 (1973). The curve represents an eyeball fit to their data with typical errors of 10 to 15%.

[16] S. J. Barish *et al.*, Phys. Rev. D 9, 2689 (1974).

[17] We have also fitted the data points versus n_- and obtained $\alpha = 0.20 \pm 0.37$, $\beta = 0.071 \pm 0.025$.

[18] G. H. Thomas, Phys. Rev. D 8, 3042 (1973).

[19] We have also fitted the data points versus n_- and obtained $\alpha = 1.36 \pm 0.33$, $\beta = 0.68 \pm 0.13$, in agreement with the values quoted by F. T. Dao and J. Whitmore, Phys. Lett. 46B, 252 (1973).

[20] A. Arneodo and J. Kubar-Andre, Nucl. Phys. B77, 309 (1974).

[21] We would like to thank R. Singer for his assistance in making the π^+ and π^- data for this exposure available to us. It should also be noted that the available data consisted of only half (4200 events) of the total number of interactions found. Each track was therefore weighted by the fraction of events measured in a particular topology compared to the total found.

[22] H. Bøggild *et al.*, Nucl. Phys. B72, 221 (1974).

[23] G. I. Kopylov, Phys. Lett. 41B, 371 (1972).